PERGAMON

International Journal of Heat and Mass Transfer 41 (1998) 3817–3828

International Journal of HEAT and MASS TRANSFER

On a physically-realizable benchmark problem in internal natural convection

W. H. Leong[1], K. G. T. Hollands*, A. P. Brunger[2]

Solar Thermal Research Laboratory, Department of Mechanical Engineering, University of Waterloo, Waterloo, Ontario, Canada N2L 3G1

Received 18 September 1997; in final form 23 February 1998

Abstract

A new natural convection 'benchmark problem' for validating CFD codes is defined. In the subject problem, a cubical air-filled cavity, tilted at 0, 45°, or 90°, has one pair of opposing faces at different temperatures, T_h and T_c, respectively, the remaining faces having a linear variation from T_c to T_h. In contrast to some other benchmark problems, this problem is physically-realizable. Experimental techniques to establish the thermal boundary conditions and to measure the Nusselt number to 1% accuracy are reported. Measured Nusselt numbers at Rayleigh number equal to 4×10^4 are shown to agree with CFD predictions to within $\pm0.3\%$.

Nomenclature

A_{hp} area of the heat plate
c_p specific heat of air at constant pressure
e emf of the heat flux meter
f function representing the variation of specified air properties due to temperature and pressure deviations from their reference values
$\boldsymbol{g}$ acceleration due to gravity
k air thermal conductivity
L distance between the hot and cold faces of the cubical cavity (see Fig. 1)
M number of measurements in a set of experiments to measure the same Nusselt number
n local slope of graph of $\log Nu$ vs. $\log Ra$
Nu Nusselt number, $=1+q_{conv}/(k\Delta TL)$
P air pressure
q heat flux; with no subscript, q is the total heat flux (convection, conduction, and radiation) across the cubical cavity from the hot to the cold plate
R gas constant for air
Ra Rayleigh number, $=\boldsymbol{g}\beta\Delta TL^3c_p\rho^2/\mu k$
t thickness of the sidewalls of the cubical cavity
t Student t multiplier at the 95% confidence level with $M-1$ degrees of freedom
T temperature (K)
V voltage measured across the terminals of the heater embedded in the heater plate
U experimental uncertainty
Z air compressibility.

Greek symbols

α proportionality constant between e and q_b
β coefficient of thermal expansion of air
ΔT T_h-T_c
$\Delta T'$ temperature difference across the heat flux meter
μ air viscosity
ρ air density
φ angle of tilt of hot face of cavity from horizontal (see Fig. 1).

Subscripts

b pertaining to the back plate
B due to bias error in a measured or calculated quantity
c pertaining to the cold plate, or pertaining to constant air properties

* Corresponding author. Tel.: 001 519 888 4053; fax: 001 519 746 0852; e-mail: kholland@solar1.uwaterloo.ca

[1] Present address: Hatch Associates, 2800 Speakman Dr., Sheridan Science and Technology Park, Mississauga, ON, Canada L5K 2R1.

[2] Present address: National Solar Test Facility Canada, ORTECH Corp., 2395 Speakman Dr., Sheridan Science and Technology Park, Mississauga, ON, Canada L5K 1B3.

0017–9310/98 $19.00
PII: S0017–9310(98)00095–7

conv due to convection only
e electrical heating
h pertaining to the hot plate
I index integer
j pertaining to a joint between the sidewall and either the hot or cold plate
k pertaining to the air thermal conductivity
m mean, or pertaining to the group $(\beta T_m c_p/(Z^2\mu k))$
o evaluated at reference temperature $T_o = 300$ K and reference pressure $P_o = 1$ atm
R due to random error
s quantity pertaining to stationary air conditions, or CFD simulated value
v pertaining to variable air properties.

Superscript
* relating to a special nominal value of the Ra, like 10^4, 10^5, 10^6, etc.

1. Introduction

Workers in computational fluid dynamics (CFD) have frequently emphasized the importance of benchmark problems. Once a benchmark problem has been solved to the satisfaction of all concerned, it can serve as a reference point for code development and validation: if the code functions well on the benchmark problem, it should also function well on other closely-allied problems. Ideally, a benchmark problem should be capable of simple statement, and yet it should challenge the more sophisticated codes. An additional requirement would also seem to be desirable: the problem should be physically-realizable in the laboratory.

This latter requirement has not always been satisfied by the popular benchmark problems. A case in point is the problem in natural convection first enunciated by de Vahl Davis [1]: namely the 2-D flow of air in a square cavity with adiabatic top and bottom walls and isothermal sidewalls. Le Quere [2], who has provided some of the most extensive solutions, noted that "we are fully aware of the fact that, for several reasons, this problem could ultimately prove to be without physical meaning". There are two good reasons for this lack of physical meaning. First, the adiabatic boundary conditions imposed on the top and bottom walls is impossible to realize for air-filled cavities (see, for example, ElSherbiny et al. [3]). Second, the 2-D flow could easily be unstable to 3-D perturbations—a condition that Penot et al. [4] have already demonstrated for a cavity of aspect ratio 4; if this is the case, the problem would lose its physical meaning.

Despite its non-physical nature, the square-cavity problem has served as a valuable concept in CFD development. Interestingly, its lack of experimental confirmation (which follows from this non-physical nature) does not appear to have raised any particular inhibitions in its use. And while there may be good mathematical reasons for this, there are also very good reasons why future natural-convection benchmark problems should be physically-realizable, so that measurements can be made. There may be, for example, some physical aspect that is missing in the fundamental equations: a case in point would be the 3-D nature of what was taken to be a 2-D problem. Even given the correctness of the mathematical model, some aspect of the flow may be missed in the solution, or the flow may be bistable and the code is converging on only one of the two solutions. The main area, however, where experimental measurements on benchmark problems would be useful is in transition and in fully-turbulent flows. Outside of direct numerical simulation, it is going to be necessary to model the turbulence in some way, and since modelling laws for buoyancy-driven turbulence are still in their early stage of development, one cannot be at all sure about the accuracy of the time-averaged equations, and the need to test solutions against experimental measurements becomes paramount.

There have been several comparisons in the literature of computed and measured results for fluid flow and heat transfer in square- or cube-like cavities [5–11]. The common finding, however, is that close agreement is not found because of the lack of correspondence between the simulated and experimental side wall boundary condition. The exception is the work of Hamady and Lloyd [9], who achieved agreement ($\pm 3\%$) for the Nusselt number, but they achieved this by using, for the boundary condition the CFD model, the experimentally-measured sidewall temperature distribution. While this close comparison constitutes useful knowledge, the method (which for a 3-D cavity would require the specification of the temperature of every point on the sidewalls) is not entirely consistent with the basic idea of a benchmark, in which the model should preferably be simply-stated and independent of any experimental measurements.

Because of the already existing history of the square-cavity benchmark problem, it would seem wise to build the new, physically-realizable problem on that foundation. The first part of this paper is about defining a suitable, physically-realizable problem. It is concluded that the most suitable problem is the natural convection of air in a cube with two opposing faces isothermal and the remaining four walls having a linear temperature variation from the cold face to the hot face—as shown in Fig. 1. We define, in fact three benchmark problems: one with hot and cold faces vertical (as in the square-cavity problem), one with them horizontal, and one with them inclined at 45°. An apparatus built up to realize the specified problem is described, and the practical achievement of the linear profile is demonstrated. It was decided that, for this particular apparatus, the average Nusselt number

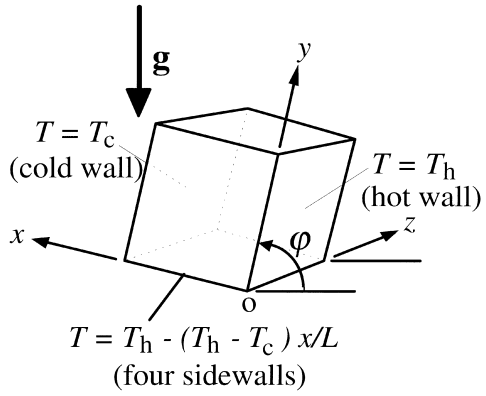

Fig. 1. Sketch defining the cubical cavity benchmark problem.

should be the measured parameters of the flow, and that the accuracy in this measurement needed to be about 1% or better, if the results are going to be useful for testing the codes. The present experiment achieved this accuracy, as will be clearly demonstrated in this paper at a Rayleigh number of 40 000. Because of length limitations, the set of results at higher Rayleigh numbers cannot be given in the present paper, whose contribution is to lay out the benchmark problem and to demonstrate its physical nature. The benchmark results at higher Rayleigh number are left for a companion paper.

2. Definition of the benchmark problem

We take as our starting point the 2-D square-cavity problem, which was not physically achievable because the 2-D assumption and the adiabatic sidewall boundary condition. (For convenience, the walls connecting the two isothermal surfaces of the cavity will be called 'sidewalls' regardless of the orientation of the cavity.) Replacing the air by a higher-conductivity fluid would make it easier to insulate and therefore to approach the adiabatic condition. On the other hand, there are at least three important advantages to keeping to (dry) air as the fluid. First it turns out that uncertainties in the thermophysical properties of the fluid are a main source of error, and despite its multicomponent nature, the properties of dry air are well-established and known to a greater precision than those of any fluid (including any of the pure gases). Second, with air it is possible to readily change the Rayleigh number by changing the air pressure, meaning that a single physical model can cover an extremely wide range in Rayleigh number [12–14] and the temperature difference can be maintained constant, which has certain benefits in the heat transfer measurement [14]. Third, the Prandtl number for air is relatively insensitive to temperature, meaning that experiments can be carried out at various temperature levels without confounding the result by introducing a third variable.

Despite the advantages of using air, one may still want to examine the option of changing the fluid to one of higher conductivity (a liquid), making it easier to insulate. One finds, however, that in view of the need to ensure that the properties are known with high accuracy, water is about the only suitable liquid option. With water one would have to build a different model for every integer power of 10 in Rayleigh number, and in order to keep the Prandtl number of the experiments constant to within say 10%, the average fluid temperature would have to be kept the same for all experiments, to within about 3 K. Moreover, while the conductivity of water is substantially higher than that of air, in practice it is still very difficult to insulate to the degree that would be required. The better insulation materials have a conductivity that is only about one-tenth that of water, instead of the one-hundredth that would be really required. Also, the container walls will generally have a conductivity comparable to that of water. (Vacuum insulation requires a thick or a metallic wall to withstand the pressure forces, and this is not compatible with the adiabatic condition—it is not sufficient merely to prevent heat loss to the environment; heat transfer through the walls to the hot and cold plates must also be prevented.) These arguments apply in fact to almost any liquid other than the liquid metals, which are unsuitable for other reasons.

Returning now to considering air as the fluid, an alternative boundary condition that is compatible with air is the specification of a linear temperature profile from hot to cold face. This well-recognized boundary condition (sometimes called the perfectly-conducting side-wall condition) is simply-stated, easily programmed and capable of being established in the laboratory, as will be demonstrated later.

The other aspect of the square-cavity problem that makes it nonphysical is its 2-D character: any real problem entails the possibility of motion in the third direction. As opposed to the situation existing when De Vahl Davis first proposed the square-cavity problem, 3-D codes are now very common. Thus including the third dimension in the benchmark problem is not only possible but preferred. The question remaining is how far the cavity should be made to extend in the third direction: an infinite distance is not practical. A suitable and simply-stated finite distance is the length of the side of the original square cavity, leading to the cubical cavity. The linear temperature-profile boundary condition can be extended to apply to the two added walls as well.

This defines the physically-realizable benchmark problem (now called the cubical cavity problem) as the one shown in Fig. 1, that is, except for the question of the orientation of the cube—see Fig. 1. The square cavity problem defined by De Vahl Davis [1] had the isothermal

walls vertical (i.e., tilt angle $\varphi = 90^\circ$). This avoided the instability and generally complex flow known to exist in the case where $\varphi = 0^\circ$—the classical layer of fluid heated from below, which, for example, is subject to bifurcation. But modern codes can handle this situation as well. It is proposed that three cubical benchmark problems be defined: one with $\varphi = 90^\circ$ (heating from the side), one with $\varphi = 45^\circ$ (oblique heating), and one with $\varphi = 0^\circ$ (heating from below). The oblique heating case will allow the study of a problem blending the characters of the other two orientations, which are know to have quite different flow structures.

There are several possibilities for the measured parameter of the benchmark problem: temperatures at specified points, maximum velocity, etc. Enforcing the linear-temperature-profile boundary condition will make some choices (e.g. those involving flow visualization) difficult (although not impossible). In the present work the relevant measured quantity will be the average Nusselt number. This measurement has a long history and should be measurable with excellent accuracy. It responds to the whole flow—and therefore is not a quirk of a particular region which may be highly variable in time as the flow flips from one mode to another. It is, however, recognized that, the average Nusselt number may be insensitive to details, so agreement with CFD simulation need not ensure that the details of the simulation are correct [15]; other choices, such as point-by-point measurements of the velocity and temperature fields would certainly be more sensitive. At the same time, agreement with the more easily measured average Nusselt number is a sine qua non of any simulation code.

This agreement need only be within the experimental error of the experiment, and this raises the issue of the required accuracy of a benchmark measurement. To be useful for benchmark work, the measured Nusselt number must not only be very close to the true one, it must also be within some known tolerance of the true one. As the goal of the present experiment, we set an experimental uncertainty of 1% in the Nusselt number. It was felt that this is small enough to meet the requirements of the CEF modellers, yet large enough to be achievable in the laboratory—although it substantially exceeds the accuracy normally achieved in natural convection experiments.

3. Experimental design

General Layout: shown in cross-section in Fig. 2, the laboratory model of the cubical cavity had the side-length L nominally equal to 127 mm (5 in). Insulated with 100 mm of fiber-glass, the model contained four main parts: a heat flux meter, an electrically-heated plate, and two matching half-cubes—or 'hemi-cubes,' which joined along the parting line shown on the figure to form the complete cube. The 'hot-plate' part of the cube was heated, and the 'back-plate' part cooled, by two separate streams of circulating water passing through tubes soldered to their rear faces. Measured at the cold end of the cavity, the heat flow was determined using a variation of the hybrid method described by Hollands [13, 14]. This method incorporates the heat flux meter and the electrically-heated plate, which in this particular instance was also the cold plate at T_c.

Achieving the Linear Profile: we describe first those aspects of the experimental design that were aimed at maintaining the linear temperature distribution in the sidewall part of the cube. One aspect of this was the above-mentioned choice for the location of the parting line: any heat transfer perpendicular to this edge would be in direct conflict with the linear temperature requirement, because contact resistance would cause a temperature jump across the parting line. In the location chosen for the parting line, no such heat transfer occurs, and there is no temperature jump. After assembly, 6 mm wide strips of copper foil with adhesive backing were run along the parting line on the outside, to close off the cavity.

The choice for the thickness t of the sidewalls, namely 3.18 mm, was made after a preliminary analysis, in which the sidewall had been treated as a fin with natural convection and radiation assumed on the face looking into the cavity, an appropriate loss coefficient to the environment on its opposite face, and the boundary condition at the ends set at $T = T_h$ at $x = 0$, and $T = T_c$ at $x = L$. With $t = 3.18$ mm, the maximum departure from linearity was conservatively estimated to be $\pm 0.2\%$ of the overall temperature difference $\Delta T = T_h - T_c$, and this was judged to be sufficiently close to the linear profile. With this setting for t, the amount of heat conducted through the sidewalls was from 100 (at $Nu = 100$) to 10 000 (at $Nu = 1$) times as great as the heat transfer going through the air in the cavity. This meant that the convection have virtually no effect on the temperature distribution inside the sidewalls.

When the model was built up along these lines and tested, a substantial constriction resistance was discovered at the joint between the hot plate and the sidewall and that between the back plate and the sidewall, as evidenced by the observation that the temperature T_{jh} at the former joint was different from the hot plate temperature T_h, and the temperature T_{jc} at the latter joint was different from the cold back-plate temperature T_{bc}. (Here T_h and T_{bc} refer to the plate temperatures far from the joints.) A detailed conduction analysis of the hot plate and the cold back plate [16] confirmed that the observed temperature difference was essentially all attributable to the constriction resistance and occurred within a short distance (about 3 mm) from the joint. The differences were of the order of 4% of the overall ΔT, which, while small, was not considered to be compatible with the design accuracy of the experiment, and a solution to the problem had to be found.

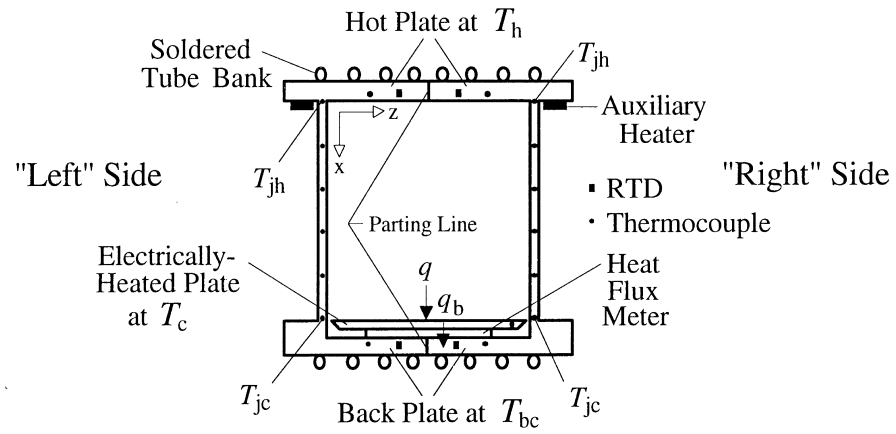

Fig. 2. Sketch of experimental apparatus in central cross-section.

When the test that discovered the constriction resistance was first being carried out, the hot water was circulated to the end containing the electrically-heated plate and the heat flux meter—which is the normal configuration for the hybrid method and the one we had expected to use here. Part of the solution to the constriction resistance problem was to switch the circulating water flows and then, for each heat flux measurement, to adjust the electrical heating until the cold plate (i.e., the electrically-heated plate) was at the same temperature as the local joint temperature T_{jc}. (Normally, in the hybrid method, it would have been adjusted until the electrically-heated plate was at the same temperature as the back plate.) This removed the temperature jump 'seen' by the gas in the corner cavity, and yet it was still basically consistent with the hybrid method, as will be discussed shortly. The second part of the solution was to insert an auxiliary heater at the joint between the sidewall and the hot plate, as shown in Fig. 2. The heater consisted of a 20 mm wide copper strip (having right angle corners to conform to the square hot plate) in which was imbedded a nichrome wire. The heater was thermally-bonded to the hot plate within 1 mm of the joint, at the location shown in the figure. (Because of the presence of the parting line, the auxiliary heater had actually to be made up in two symmetric parts, one for each hemi-cube.) As had been predicted by a detailed conduction analysis of the hot plate [16] and confirmed by experiments, a proper level of auxiliary electrical heating could be found to reduce the temperature jump at this end of the cavity to less than 0.1% of the overall ΔT. Moreover, the amount of electrical heating required was unaffected by the convection inside the cavity, so it could be set once and for all, once the plate temperatures had been fixed.

Pressure/Density Variation Technique: a function of ΔT, L, and ρ, the Rayleigh number can in principle be varied by varying any of these three quantities. On the other hand, to avoid excessive nonuniformity of fluid properties, ΔT can be varied only over a rather limited range, and varying L requires the construction of several models as well as presenting other problems [17]. The remaining alternative is to vary the density by varying the pressure, and this is what was adopted in the present experiments.

The model was mounted in a pressure vessel, that, along with its ancillary equipment, was developed by Shewen [18] and subsequently used by Moore and Hollands [19], and Karagiozis et al. [20], among others. The vessel can maintain pressures ranging from 0.1–1140 kPa. The pressure-controlling solenoid valves, the tilting mechanism for the model, and data acquisition system are computer-controlled. Air from the University's compressed air lines was used as the fluid. With a humidity ratio of less than 2.5 g of water vapour per kg of dry air, it had properties essentially the same as those of dry air, and it was treated as such for property evaluation. Given the model built up for the present experiments and given the above-stated pressure range of the vessel, the range of Ra that could be covered was from about 100 to about 2×10^8. On the other hand, at pressures below about 10 kPa, rarefied gaseous conduction effects—not included in the theoretical models of interest, which assumed the gas was in a continuum—began to influence the heat transfer, so the practical range of Ra was actually from about 10^4 to 2×10^8.

Heat Transfer Measurement Technique: both the heat flux meter and the electrically-heated plate (which was also the cold plate in the present experiments) had been used previously in other published experiments, and as such are described in more detail elsewhere [13]. With thickness of 3.21 mm and constructed of copper with chamfered edges as shown, the electrically-heated plate had been previously shown to take up a temperature distribution uniform to within about 0.01 K in the

environment it experienced in the model. Four threaded rods projecting from its rear face passed through holes in the back plate. Nuts and plastic washers on these rods permitted the cold plate to be snugged up tightly against the heat flux meter, which had been greased prior to assembly. An air gap (average width = 0.36 mm) was left between the edge of the electrically-heated plate and the sidewall. The heat flux meter, a 3.30 thick by 105 mm diameter disc, has an output *emf*, e, that is a very sensitive measure (sensitivity equal to 17 mV K^{-1}) of the temperature difference $\Delta T'$ across it. A steady-state heat balance on the cold plate gives

$$q = q_b - q_e \tag{1}$$

where q is the sought heat transfer across the cavity (including radiation), q_e is the electrical power input to the cold plate (determined from the relevant voltage drop V and current I) and q_b is the heat transfer from the cold plate. Most (but certainly not all) of q_b passes through the heat flux meter; the rest travels through the air gap between the electrically-heated plate and the back plate and (in a small amount) through the threaded rod and electrical wires attached to the back of the electrically-heated plate. Both the *emf* output of the heat flux meter, e, and q_b are proportional to the temperature difference $\Delta T'$ between the cold plate and the back plate. It follows that q_b and e will be proportional to each other, meaning that q_b will equal αe, where α is a proportional constant. It should be noted the proportionality will apply even though the back plate's near-isothermality does not extend to the constriction-resistance region near the joint where the sidewall meets the back plate; the proportionality requires only that the shape of the temperature profile on the back plate be constant, independent of q. (It should also be noted that the proportionality will still apply even though q_b includes heat transfer passing through the electrical wires and the threaded rods, because the other ends of these wires and rods were only in thermal contact with the back plate.) An in situ calibration [16] was used to determine proportionality constant α. Equation (1) can now be re-expressed in terms of measured quantities e, V, and I:

$$q = \alpha e - VI. \tag{2}$$

To start a measurement of the convective component q_{conv} of the heat transfer across the cavity, the model was first put in the heated-from-above orientation (i.e., $\varphi = 180^\circ$), where the air in the cavity is stationary, there being no convection. The heat transfer q at this orientation consists of radiation and pure gaseous conduction. We denote this 'stagnant condition' by the subscripts s. Thus

$$q_s = \alpha e_s - (VI)_s. \tag{3}$$

During this measurement, the electrical heating was adjusted until the temperature T_c of the cold plate was the same as the temperature T_{jc} at the joint, thus eliminating the temperature jump discussed previously. Then the model was rotated to the orientation of interest, and the measurement repeated. The convective heat transfer q_{conv} was then obtained by subtracting the heat transfer q_s from the heat transfer q measured at the orientation at hand, Thus,

$$q_{conv} = [(VI)_s - (VI)] - \alpha(e_s - e). \tag{4}$$

This is the equation from which q_{conv} was determined, to be entered into the Nusselt number. One of the basic assumptions of this technique was that the air really was stationary in the heated-from-above orientation. To test this assumption, the heat transfer q_s in this orientation was measured as a function of pressure; if there was any convective motion happening, the heat transfer should certainly vary with the Rayleigh number and hence with the pressure. The finding was that the heat transfer was essentially independent of pressure for pressures greater than about 10 kPa, which would correspond to a Rayleigh number greater than about 10^4. (The reduced heat transfer that was observed at lower pressures was shown to be attributed to rarefied, or non-continuum, effects.) It was therefore concluded that the assumption was a valid one. It was also concluded that Nusselt number measurements at Ra less than about 10^4 may not corresponds to the continuum regime and should therefore be discounted.

In using the above method, it was often too time-consuming to go to the heated-from-above orientation to get $(VI)_s$ and e_s for every q_{conv} measurement. Since the heat transfer in the heated-from-above orientation was essentially independent of pressure, we tentatively concluded that one needs to measures $(VI)_s$ only at one or two pressures in the continuum regime, opening the way to a simpler, less time-consuming technique. On the other hand, equation (4) assumed that $\alpha = \alpha_s$, and so if α is a function of pressure, the simpler technique would not be valid. The pressure-dependence of α was measured (at various temperature settings) and α was indeed found to be highly-insensitive to pressure, in the continuum regime [16]. And so $(VI)_s$ and e_s had only to be determined once, for a given set-up.

Temperature Determination: a high degree of temperature uniformity of the hot and back plates was designed into the apparatus, through the choice of the plate thicknesses, the circulation rate of the water passing through the tubes, and the tube spacing. A thermal analysis [16], which assumed the highest Rayleigh number as a worst case and allowed for heat loss to the ambient, indicated that the plate temperatures should be uniform to within about ± 0.035 K. The temperatures of the hot plate and the back plate were measured using four platinum resistance temperature detectors (RTDs). Two RTDs were embedded in each of the two plates—one on each side of the parting line—and the temperature of each plate was calculated as the average of these two

measurements. The RTDs had been calibrated against a platinum resistance thermometer having an accuracy of 0.01 K. The remaining temperatures were measured with Type-T thermocouples, which are calibrated along with the RTDs, and which had their reference junction near one of the RTD's. Twelve thermocouples, six on each side of the parting line of the model, were used to measure the sidewall temperature profile. One junction of each thermocouple was on the sidewall and the other was on either the hot or back plate—whichever one was closer to the corresponding junction in the sidewall. The temperature of the electrically-heated plate was measured using a calibrated thermocouple embedded in the plate.

Procedure: once a particular setting of the variables (pressure, tilt angle, temperatures, etc.) had been made, the value of α was determined and a search was initiated to find the power to the electrically-heated plate that would make the temperature difference T_c minus T_{jc} be zero (within 0.025 K). This was done with a microcomputer programmed to change the supply voltage V from a pre-set upper bound to a pre-set lower bound whenever the temperature difference changed sign. The relative time at each bound was observed, and based on this information, the bound settings were gradually altered and brought closer together until the required power was found. Then a roughly one half hour measurement period was entered into during which 512 measurements were made of each of V, I, e, the temperatures, and the pressure, the results averaged. From this data the Nusselt number and the Rayleigh numbers were calculated from

$$Nu = 1 + \frac{((VI)_s - VI - \alpha(e_s - e))L}{k_o \Delta T A_{hp} f_k(T_m, P} \tag{5}$$

$$Ra = \frac{\boldsymbol{g} c_{po} \Delta T L^3 P^2}{Z_o^2 \mu_o k_o R^2 T_m^3} \cdot f_m(T_m, P) \tag{6}$$

where the subscript 'o' on a property means the value of a property evaluated at reference temperature $T_o = 300$ K and reference pressure $P_o = 1$ atm, and the functions $f_k(T, P)$ and $F_m(T, P)$ account for the variation of k and the group $(\beta T_m c_p/(Z^2 \mu k))$ with temperature T and pressure P. They typically ranged from about 0.95–1.023 in the experiments to be reported here. Drawn from the literature, equations for these functions are given by Leong [16].

Error Analysis: the multiple-sample method of Moffat [21] is adopted for the error analysis, but with a minor variation described shortly. In Moffat's method, one repeats similar experiments (say M in all) and then one estimates the overall random error E_R from the standard deviations of the observed results. The fixed (or bias) error E_B is established separately for the accuracy of instruments and similar considerations. The total uncertainty U_Y is then calculated as the root mean square of the fixed and random errors: $U_Y = (E_R^2 + E_B^2)^{1/2}$. It is assumed, in the method, that one is trying to determine the error in a quantity Y (for example, Y could be the Nusselt number) that is not measured in itself but is calculated from measurements of the set of measured variables: X_i with $i = 1, 2, \ldots, N$ using a function $Y = Y(X_1, X_2, \ldots, X_N)$. An example of such a function is equation (5) above with $X_1 = V$, $X_2 = I$, $X_3 = L$, etc. The fixed error E_B in Y is obtained from

$$E_B = \left[\sum_{i=l}^{N} \left(\frac{\partial Y}{\partial X_i} \cdot B_i \right)^2 \right]^{1/2} \tag{7}$$

where B_i is the bias error in X_i, and the random error E_R from

$$E_R = t \left[\sum_{i=l}^{N} \left(\frac{\partial Y}{\partial X_i} \cdot S_i \right)^2 \right]^{1/2} \tag{8}$$

where t is the Student t multiplier at the 95% confidence level with $M-1$ degrees of freedom and S_i is the standard deviation of the set of M measurements of X_i, there being one for each experiment.

Table 1 presents the bias errors for each X_i that enters into the evaluation of Nu and Ra. Details of their determination are given by Leong [16]. In certain cases (e.g. for L, ΔT, and A_{hp}), the error incudes a contribution associated with the spatial variation of a subject quantity. For example, in addition to thermocouple calibration errors and contact *emf*s, the B_i corresponding to ΔT takes into account that ΔT is not truly uniform across the cavity, because of the afore-mentioned temperature non-uniformities. It is recognized that, though included in Table 1, the fluid properties k_o, μ_o, Z_o and c_{po}, were not actually measured in the M experiments in question; nevertheless they are included because their uncertainties contribute to the bias error in Nu and Ra in the manner given by equation (7). The bias errors in $f_k(T_m, P)$ and $f_m(T_m, P)$ were assumed to arise only from the bias errors in T_m and P; that is, the parameters in their equations were assumed to be free of error.

As mentioned earlier, we actually used an altered form of Moffat's multiple-sample method. The alteration was motivated by the fact that Moffat's method requires that all the X_i should have the same nominal values in all of the M experiments, whereas in the present experiments, different nominal values are used for several of the variables—namely ΔT, P, and T_m. The experiments are done in such a way, however, that the same nominal value of Ra applied in all the experiments, so that, one could expect all the Nusselt numbers to be the same, if there were no random errors. While in spirit this is very close to (and indeed is an extension of) Moffat's basic idea, it does mean that equation (8) cannot be used for determining E_R. One can show, however, that subject to standard assumptions on the nature of the errors (that they are small and independent) the following equation gives the same e_R as equation (8):

Table 1
Errors in measured quantities, X_i

Index i	Quantity X_i	Unit	Nominal value(s) or range of X_i	Bias limit $B(X_i)$
1	VI, $(VI)_s$	W	$0 < VI < 1.24$	$0.0003VI$
2	e, e_s	mV	$6.5 < e < 31$	$0.00015e$
3	ΔT	K	4, 5, 6, 10	$\sqrt{3\times10^{-5}\Delta T^2+5\times10^{-4}}$
4	P	Pa	$P < 10^4$	$\sqrt{(5\times10^{-4}P)^2+1.09}$
			$10^4 < P < 10^5$	$\sqrt{(5\times10^{-4}P)^2+64.4}$
			$P > 10^5$	$\sqrt{(5\times10^{-4}P)+6400}$
5	T_m	K	297, 307	$\sqrt{(7\times10^{-6}\Delta T)+6\times10^{-4}}$
6	α	W mV^{-1}	0.0390	0.005α
7	L	m	0.1272	0.00008
8	A_{hp}	m^2	1.623×10^{-2}	0.00009
9	R	J kg^{-1} K^{-1}	287.1	$0.0003R$
10	$\boldsymbol{g}$	m s^{-2}	9.80379	0.00010
11	Z_o		0.999702	0.00086
12	k_o	W m^{-1} K^{-1}	0.02614	$0.01k_o$
13	μ_o	N s m^{-2}	1.846×10^{-5}	$0.005\mu_o$
14	c_{po}	J kg^{-1} K^{-1}	1006.69	$0.0013c_{po}$
15	n		0.30	0.03

$$E_R = t\left[\frac{\sum_{j=1}^{M}(Y_j-\bar{Y})^2}{M(M-1)}\right]^{1/2} \tag{9}$$

where Y_j is the calculated value of Y from the jth experiment and $\bar{Y}$ is the average of the Y_j. The use of equation (9) for E_R is not restricted to there being the same nominal X_i in all experiments, and so it will be adopted for evaluating the random error.

It is common in CFD work to report the Nusselt number at a particular Rayleigh number such as 10^4, 10^5, 10^6, etc. Let this specified Ra be denoted as Ra^* and the corresponding Nu as Nu^*. The experimentalist can set the Rayleigh number to some value very close to Ra^*, but the exact number will never be precisely achieved because there will be a bias error in Ra and also because, even in the absence of bias errors, it is not normally possible to set a measured variable exactly to a specified value. All of this will cause an error in the reported Nu^*. One cannot establish this error without some estimate of how quickly Nu is changing with Ra. It is widely recognized, however, that the slope of a graph of log Nu vs. log Ra is a slowly varying function of Ra. This implies that provided we are looking at small differences in Ra and Ra^*—normally the case in error analysis—then the first two terms will suffice in the Taylor Series expansions in log Ra of log Nu about log Ra^*. If the resulting equation for log Nu is exponentiated and solved for Nu^*, there results

$$Nu^* = Nu(Ra^*/Ra)^n \tag{10}$$

where n is the slope of the logarithmetic plot. Substituting equations (5) and (6) for Nu and Ra into equation (10) gives the equation for Nu^* in terms of the X_i and n, and so by treating Y as Nu^* in equation (7) and (9) the error in Nu^* can be established. This process will however require a fixing of the index n: n can be estimated from the value of Nu at values of Ra^* in the vicinity of the Ra^* of current interest. For example, if Ra^* is 10^5, n can be estimated from measurements of Nu and $Ra = 10^4$ and 10^6. This estimate will be in some (bias) error, and so n must be added to the list of the set X_i determining the errors in X_i. The uncertainty in n given in Table 1 is conservatively large, yet it did not contribute significantly to the uncertainty in Nu^*.

4. Results

The Temperature Profile in the Sidewalls: Fig. 3 shows the measured temperature distribution measured at the sidewalls (experimental points), with desired straightline profile shown as a solid line. There was a row of thermocouples on each hemi-cube, and so two plots are shown, one for each side. The observed points deviate from the straight line by about ±0.05 K, which was just slightly less than the measurement uncertainty in temperature. In this particular experiment the Rayleigh number was approximately 10^7 and angle φ was 90°, but similar linearity was observed at other values of Ra and φ.

Critical Rayleigh Number Determination: as a second

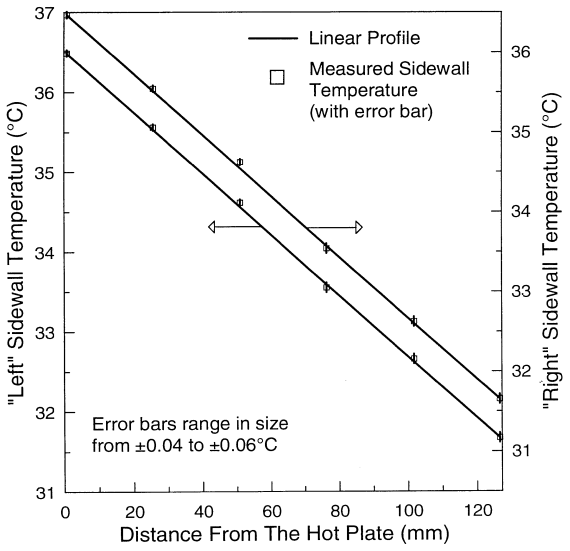

Fig. 3. Plot of the temperature distribution on the side-wall demonstrating the required fidelity to the sought linear profile.

check of the apparatus, the critical Rayleigh number Ra_c in the $\varphi = 0^\circ$ (heating from below) was measured and the result compared to the theoretical value of Ra_c for the linear temperature profile, which is 6974 (Catton [22]). This check also tested the linearity of the sidewall temperature profile, since Ra_c is quite dependent on the nature of the sidewall boundary condition—e.g., for the adiabatic sidewall Ra_c is equal to 3446. The experimental method of Hollands and Konicek [23] was used for the Ra_c determinations, which were carried out with $\Delta T = 9.5$ K and again with $\Delta T = 5.4$ K. In both cases T_m was 295 K. The results were as follows: at $\Delta T = 9.5$ K, Ra_c was measured to be 6969 ± 144; at $\Delta T = 5.4$ K, Ra_c was measured to be 7058 ± 119. The theoretical value of 6974 is well within experimental error of both of these experimental values.

Results of Error Analysis at $Ra^* = 40\,000$: a set of experiments were made at Ra nominally equal to 40 000, at each of the tilt angles: $\varphi = 0$, 45°, and 90°. In all, 48 experiments were performed: 18 at $\varphi = 0^\circ$, 18 at $\varphi = 45^\circ$, and 12 at $\varphi = 90^\circ$. For each of the $\varphi = 0^\circ$ and $\varphi = 45^\circ$ angular settings, the experiments covered six different combinations of ΔT and T_m, namely the six permutations of the $\Delta T = 4.5$ K, 6.2 K, and 9.7 K with $T_m = 298$ K and $T_m = 308$ K. For the $\varphi = 90^\circ$ angular setting, they covered the same set, except the two permutations of $\Delta T = 6.2$ K and 9.7 K with $T_m = 298$ K were not done. For each combination, the pressure was adjusted to one of three slightly-different values, all three of which brought the Rayleigh number to a value between 39 400 and 40 600, and an experiment was performed at each pressure setting. This completed the total set of 48 experiments.

Table 2 gives the results in the first five items. Item 1 reviews the number of experiments at each φ. Item 2 gives the measured Nu^*, calculated as the average of the M measured values of Nu^*; it is the value that is to be compared with the numerically simulated Nusselt number at $Ra = 40\,000$. Items 3 and 4 give the random and bias errors, E_R and E_B, in Nu^* calculated using equations (7) and (9) with Y equal to Nu^*. Item 5 is the uncertainty U_{Nu} in Nu^*, taken as the square root of the sum of the squares of E_B and E_R. Values given in brackets in Items 3, 4, and 5 express the corresponding errors as percentages of Nu^*. It would appear from these entries that the goal of measuring the Nusselt number within a projected error of 1% has been achieved.

Comparisons with CFD Simulations at $Ra^* = 40\,000$: at a Rayleigh number as low as 40 000, CFD simulations of steady laminar flow can be resolved to high accuracy, and there is no reason to expect turbulent or unsteady flow, even at $\varphi = 0^\circ$ [6, 9]. Thus a comparison of such simulations with the experimental values of Nu^* at this Ra^* will form the final check of the apparatus and of the method of estimating errors. The Appendix gives the details of the CFD simulations that were carried out to calculate simulated values (denoted Nu_s^*) of Nu^*, to be compared with the experimental values. The uncertainties in Nu_s^* were an order of magnitude smaller than the experimental uncertainties, so for practical purposes Nu_s^* will be treated as exact.

In the first round of the CFD simulations, the fluid properties were treated as invariant with temperature, and the results, denoted $Nu_{s,c}^*$ are given as Item 6 in Table 2. They are seen to be quite close to the experimental values, but nonetheless, for two of the three angular settings, the disagreement is greater than the experimental uncertainty. An excellent single-number 'comparison-ratio' is afforded by forming the ratio, given in Item 7, which is the difference between the simulated and experimental values, divided by the uncertainty in the experimental value. This quantity would be expected to be greater than unity only 1 in 20 times, and it is seen to be greater than unity in two of the three comparisons shown.

The CFD simulations were repeated using variable fluid properties. In these simulations the values of T_m and ΔT were set at average values over the M experiments, the actual method of forming these averages will be defined later. The results, denoted $Nu_{s,v}^*$, are shown in Item 8 in Table 2. In the case of variable fluid properties, the hot and cold plate Nusselt numbers are not necessarily the same, and the results reported in Table 2 are those at the cold plate, which is where the heat flow was actually measured. Item 9 gives the comparison-ratio for this case, and the ratio is seen to be less than unity in all of the three cases. Item 10 gives the per cent difference between the experimental and (variable-property) simulated Nusselt numbers. These differences average 0.28%.

Table 2
Results of experiments and simulations at $Ra^* = 4 \times 10^4$

		φ		
n	Item	0°	45°	90°
1	No. of experiments, M	18	18	12
2	Nu^*	2.018	2.561	2.337
3	Random error in Nu^* (as % of Nu^*)	0.0083 (0.41%)	0.0174 (0.68%)	0.0068 (0.29%)
4	Bias error in Nu^* (as % of Nu^*)	0.0128 (0.63%)	0.0170 (0.66%)	0.0157 (0.67%)
5	Uncertainty U_{Nu} in Nu^* (as % of Nu^*)	0.015 (0.74%)	0.024 (0.94%)	0.017 (0.73%)
6	Simulated Nu^*, based on constant fluid props, $Nu^*_{s,c}$	1.999	2.557	2.289
7	$\frac{Nu^* - Nu^*_{s,c}}{U_{Nu}}$	1.24	0.16	2.81
8	Simulated Nu^*, based on variable fluid props, $Nu^*_{s,v}$	2.027[a]	2.568[a]	2.340
9	$\frac{Nu^* - Nu^*_{s,v}}{U_{Nu}}$	−0.59	−0.29	−0.18
10	$\frac{Nu^* - Nu^*_{s,v}}{Nu^*}$, %	0.45%	0.27%	0.13%
11	$\overline{(\Delta T/T_m)}$ = average of $(\Delta T/T_m)$ over M experiments	0.0224	0.0224	0.0203

[a] Based on extrapolation/interpolation from conditions with $(\Delta T/T_m)$ was slightly different from the average $(\overline{\Delta T/T_m})$ of the experiments.

It is clear from these results that variable fluid property simulations are going to be required to get values that are within experimental error of the experimental values. This means that Nu is a function of another dimensionless group, in addition to Ra and Pr. A suitable group would seem to be the ratio $\Delta T/T_m$. For very small values of this ratio, the constant property simulations should yield accurate values, but even with the small ΔTs used in the present experiments, this limit has not been reached. Given that the $\Delta T/T_m$ was not the same in all of the 18 or so experiments performed at a given angle, the question arises as to how one can do a single simulation to account for the multi-experiments that went into an experimental determination of Nu^*. We feel that because the difference in Nusselt number between the constant-property and variable-property solutions were very small (of order of 1%), the first term in the Taylor Series expansion of Nu^* about $\Delta T/T_m$ should be sufficient to cover the observed effect, and therefore a single simulation taken at the average $\Delta T/T_m$ in the 18 or so experiments should suffice. (An alternative would be to perform 18 simulations, and average the Nusselt numbers obtained. While this would simulate what was actually done experimentally, it would involve a very large number of simulations.) The values of $\Delta T/T_m$ for the three angular settings are given as Item 11 in Table 2. In fact, of the variable-property simulations reported in Table 2, only the simulations at $\varphi = 90°$ actually had $\Delta T/T_m$ equal to the average of the experiments. Those at $\varphi = 0°$ had the $\Delta T/T_m$ about 35% less than, and those at $\varphi = 45°$ had $\Delta T/T_m$ about 42% greater than the average values on the experiments. The values reported in the Table have been corrected for the difference on the basis of the aforementioned Taylor Series approximation for the $\Delta T/T_m$ effect.

5. Conclusions

The differentially-heated, air-filled cavity with the sidewalls having a linear temperature distribution from the cold to the hot plate can be physically achieved in the laboratory. This means that the subject cavity at any orientation can serve as the basis of a simply-stated benchmark problem for testing CFD codes, and therefore, codes can be tested against experimental results as well as against the results of other codes.

Clearly, for the experimental results to be useful, their

experimental error must be known with reasonable accuracy. Moreover, this error should be small enough for the code to be tested in a demanding way. We have shown in this paper that an error in the Nusselt number of the order of 1% or less is demonstrably achievable. The error was established using standard methods for assessing errors, and this assessment has been validated by testing against essentially exact solutions achievable at low Rayleigh number. Thus at $Ra = 4 \times 10^4$, the measured results and those obtained with a converged CFD code agree with an average deviation of 0.3%. Measurements of the critical Rayleigh number at the horizontal orientation also gave results that agree closely with the theoretical value, in this cases to within about 1%.

In order for the CFD simulations to give results that agree with the experimental results for the Nusselt number within the experimental error, the CFD code must model the way in which the fluid properties vary with temperature. This statement is true for the present experiments, even though the temperature difference was kept to a value (about 6 K) that was only about 2% of the mean of the two plate absolute temperatures. This means that the plate temperatures in the simulated problem must match those in the experiments.

The advantage to keeping to air as the fluid is that one can achieve a wide range in Rayleigh number while keeping to the same experimental model, the Rayleigh number for a given model being limited only by the maximum pressure achievable with the apparatus. In the apparatus and the model of the present experiments, one can achieve Rayleigh numbers of the order to 10^8. The Nusselt numbers at Rayleigh numbers of 10^5, 10^6, 10^7, and 10^8 will be given in a companion paper.

Acknowledgements

This work was supported by a Natural Sciences and Engineering Research Council (NSERC) Canada Scholarship to W. H. Leong, and also by a Research Grant from NSERC. We also wish to thank Marius VanReenan for his assistance in designing and trouble-shooting the apparatus.

Appendix : Description of CFD simulations

A computational code called TASCflow3D, developed by Advanced Scientific Computing Ltd, Waterloo, Ontario, Canada was used for the numerical simulations whose results are listed in Table 2. TASCflow3D uses the finite volume method to solve the three-dimensional Navier-Stokes equations and the energy equation. The Boussinesq approximation was used. Sutherland's Law was used to represent the temperature dependence of the fluid's thermal conductivity and viscosity, and an equation given by Shewen [18] was used to represent the temperature dependence of specific heat. The ideal gas law was used to represent the temperature dependence of the density and the volumetric expansion coefficient, β. Because of the symmetry of the cavity about the plane $z = W/2$ (see Fig. 1 for co-ordinate system), only half of the cavity needed to be simulated. A rectilinear grid was set up, with a power-law distribution of nodes in each of the three directions. Convergence was assumed to have been obtained when the maximum dimensionless residual in each transport equation was less than 10^{-5}. Convergence took much longer (several days) to be achieved at the $\varphi = 0$ configuration, indicating a tendency for unsteady flow at that angle, but eventually a converged solution was obtained for all three angle settings. Three different grid sizes were used: $16 \times 7 \times 15$, $30 \times 14 \times 30$, and $60 \times 28 \times 60$, each of these triplets corresponding to the number of nodes in the x, z, and y directions, respectively. Then the Repeated Richardson Extrapolation (RRE) method [24] was used to extrapolate these individual results for Nu to give the expected result for an infinite grid and this latter value was taken to be the exact answer. The numerical error in this value was taken to be one-half the difference between the result obtained with the finest grid and the RRE extrapolated result. In the constant fluid property simulation, the properties were evaluated at the mean temperature T_m, whereas in the variable property simulation the properties were calculated locally. The values of T_m, ΔT and the pressure P in the three simulations were as follows: at $\phi = 0$, $T_m = 307.8$ K, $\Delta T = 4.42$ K, and $P = 23.21$ kPa; at $\phi = 45^\circ$, $T_m = 308.8$, $\Delta T = 9.64$ K, and $P = 15.85$ kPa; and at $\phi = 90^\circ$, $T_m = 306.5$, $\Delta T = 6.11$ K, and $P = 19.85$ kPa. The corresponding Nusselt numbers for the constant property simulations were 1.9989, 2.5570, and 2.2887, respectively, while the corresponding Nusselt numbers for the variable-property simulations were 2.0179, 2.579, and 2.3400, respectively.

References

[1] de Vahl Davis G. Natural convection of air in a square cavity: a bench mark numerical solution. Int J Numerical Methods Fluids 1983;3:249–64.
[2] Le Quere P. Accurate solutions to the square thermally driven cavity at high Rayleigh number. Computers Fluids 1991;20(1):29–41.
[3] El Sherbiny SM, Hollands KGT, Raithby GD. Effect of thermal boundary conditions on natural convection in vertical and inclined air layers. Journal of Heat Transfer 1982;104:515–20.
[4] Penot F, N'Dame A, Le Quere P. Investigation of the route to turbulence in a vertical differentially heated cavity. In Proc 9th Int Heat Transfer Conf Jerusalem 1990;2:417–22.
[5] Viskanta R, Kim DM, Gau C. Three-dimensional natural

convection heat transfer of a liquid metal in a cavity. Int J Heat Mass Transfer 1986;29(3):475–85.
[6] Opstelten IJ, Henkes RAWM, Hoogendoorn CJ. On stability mechanisms of the natural convection flow in a side-heated cubical enclosure. First European Conference on Thermal Sciences 1992;3:523–9.
[7] Yguel F, Vullierma JJ. Experimental study of high Rayleigh number three-dimensional natural convection in air. In Significant Questions in Buoyancy Affected Enclosure or Cavity Flows. HTD-60, New York : The American Society of Mechanical Engineers, 1986. pp. 37–44.
[8] Lankhorst AM, Hoogendoorn CJ. Three-dimensional numerical calculations of high Rayleigh number natural convective flows in enclosed cavities. Proc 1988 National Heat Transfer Conf. New York : Heat Transfer Division, American Society of Mechanical Engineers, 1988;3:463–70.
[9] Hamady FJ, Lloyd JR. Study of local natural convection heat transfer in an inclined enclosure. Int J Heat Mass Transfer 1989;32(9):1697–708.
[10] Fusegi T, Hyun JM, Kuwahaaras K, Farouk B. A numerical study of three-dimensional natural convection in a differentially heated cubical enclosure. Int J Heat Mass Transfer 1991;34(6):1543–57.
[11] Le Peutrec Y, Lauriat G. Effects of the heat transfer at the side walls on natural convection in cavities. Journal of Heat Transfer 1990;112:370–8.
[12] Saunders OA. The effect of pressure on natural convection in air. Proc Royal Soc, Ser A 1936;157:278–91.
[13] Hollands KGT. Natural convection in horizontal thin-walled honeycomb panels. Journal of Heat Transfer 1973;439–44.
[14] Hollands KGT. Direct measurement of gaseous natural convective heat fluxes. In Shah et al. editors. Experimental Heat Transfer, Fluid Mechanics and Thermodynamics. New York : Elsevier, 1988. pp. 160–8.
[15] Ostrach S. Natural convection in cavities and enclosures. Journal of Heat Transfer 1988;110:1175–90.
[16] Leong WH. Benchmark experiments on natural convection heat transfer across a cubical cavity. Ph.D. thesis, Department of Mechanical Engineering, University of Waterloo, Waterloo, Ontario, Canada, 1996.
[17] Wilkie D. The correlation of engineering data reconsidered. International Journal of Heat Mass and Fluid Flow 1985;6(2):99–103.
[18] Shewen EC. A Peltier-effect technique for natural convection heat flux measurement applied to the rectangular open cavity. Ph.D. thesis, Department of Mechanical Engineering, University of Waterloo, Waterloo, Ontario, Canada, 1986.
[19] Moore GA, Hollands KGT. Natural convection heat transfer from a plate in a semicircular enclosure. Journal of Heat Transfer 1992;114:123–6.
[20] Karagiozis A, Raithby GD, Hollands KGT. Natural convection heat transfer from arrays of isothermal triangular fins in air. Journal of Heat Transfer 1994;116:105–11.
[21] Moffat RJ. Describing the uncertainties in experimental results. Experimental Thermal and Fluid Science 1988;1:3–17.
[22] Catton I. Convection in a closed rectangular region : the onset of motion. Journal of Heat Transfer 1970;92:186–7.
[23] Hollands KGT, Konicek L. Experimental study of the stability of differentially heated inclined air layers. Int J Heat Mass Transfer 1973;16:1467–76.
[24] Zwillinger D. Handbook of Integration. Boston : John Bartlett Publishers, 1992.